Successes and Failures of Stress Transport Closure Models

Successes of Stress Transport Closure Models

The stress transport models succeeded in predicting a number of complex flows. Examples of these are:

- Prediction of turbulence induced secondary flows in ducts.
- Prediction of turbulent wall flow with surface curvature.
- Prediction of noncoincidence of the surfaces of zero shear stress and zero mean strain in asymmetric flow.
- Prediction of the action of buoyancy forces on the structure of flow.

Failures of Stress Transport Closure Models

The stress transport models had difficulties in predicting a number of other flows. For example, unsatisfactory results were obtained in the following cases:

- Near-wake flows behind bluff bodies.
- Predictions of the rate of spread of round jets overestimated the experimental data by about 50%.
- Isotropic approximation to the processes containing pressure fluctuations predicts buoyant interactions of quite wrong magnitude in many of the stress and heat-flux component.

Higher Order Moment Closure Models

Third Order Moment and Clipping Approximation (Andre, De Moor, Lacarrere, Therry, and du Vachat, 1979)

Andre et al. (1979) described a third-order moment closure model that makes use of quasi-normal clipping approximation. They used a Quasi-Gaussian assumption for the fourth order moment as well as the Schwartz inequality to achieve closure. These are:

Quasi-normal Approximation:

$$\overline{a'b'c'd'} = \overline{a'b'}\,\overline{c'd'} + \overline{a'c'}\,\overline{b'd'} + \overline{a'd'}\,\overline{b'c'} \tag{1}$$

Schwartz Inequality:

$$\left(\overline{a'b'c'}\right)^2 \le \overline{a'^2}\left(\overline{b'^2c'^2} - \left(\overline{b'c'}\right)^2\right) \tag{2}$$

Andre et al. (1979) presented the example of a turbulent buoyant flows between two parallel plates. Assuming $U_i \dfrac{\partial}{\partial x_i} = 0$ and $U_1(z), U_2(z), U_3 = 0$, the governing equations of motion becomes:

$$\frac{\partial \overline{u_i}}{\partial t} = -\frac{\partial \overline{u_i'w'}}{\partial z} - \frac{1}{\rho}\frac{\partial \bar{p}}{\partial x_i} \qquad (\text{with } \overline{u_3} = \overline{w} = 0) \tag{3}$$

$$\frac{\partial \overline{T}}{\partial t} = -\frac{\partial \overline{w'T'}}{\partial z} \tag{4}$$

$$\begin{aligned}\frac{\partial \overline{u_i'u_j'}}{\partial t} = &-\frac{\partial \overline{u_i'u_j'w'}}{\partial z} - c_4\frac{\varepsilon}{\bar{e}}\left(\overline{u_i'u_j'} - \frac{2}{3}\delta_{ij}\bar{e}\right) - \frac{2}{3}c_5\left(\overline{u_k'w'}\frac{\partial \overline{u_k}}{\partial z} - \beta\overline{w'T'}\right)\delta_{ij} \\ &- (1-c_5)\left\{\overline{u_i'w'}\frac{\partial \overline{u_j}}{\partial z} + \overline{u_j'w'}\frac{\partial \overline{u_i}}{\partial z} - \beta\left(\overline{u_i'T'}\delta_{3j} + \overline{u_j'T'}\delta_{3i}\right)\right\} - \frac{2}{3}\varepsilon\delta_{ij}\end{aligned} \tag{5}$$

$$\frac{\partial \overline{u_i'T'}}{\partial t} = -\frac{\partial \overline{u_i'w'T'}}{\partial z} - \overline{u_i'w'}\frac{\partial \overline{T}}{\partial z} - c_6\frac{\varepsilon}{\bar{e}}\overline{u_i'T'} - (1-c_7)\left(\overline{w'T'}\frac{\partial \overline{u_i}}{\partial z} - \beta\overline{T'^2}\delta_{3i}\right) \tag{6}$$

$$\frac{\partial \overline{T'^2}}{\partial t} = -\frac{\partial \overline{w'T'^2}}{\partial z} - 2\overline{w'T'}\frac{\partial \overline{T}}{\partial z} - c_2\frac{\varepsilon}{\overline{e}}\overline{T'^2} \tag{7}$$

$$\frac{\partial \varepsilon}{\partial t} = a_1\frac{\partial}{\partial z}\left(\frac{\overline{e}}{\varepsilon}\overline{w'^2}\frac{\partial \varepsilon}{\partial z}\right) - a_2\frac{\varepsilon}{\overline{e}}\overline{u_i'w'}\frac{\partial \overline{u_i}}{\partial z} + a_{2T}\frac{\varepsilon}{\overline{e}}\beta\overline{w'T'} - a_3\frac{\varepsilon^2}{\overline{e}} \tag{8}$$

$$\begin{aligned}\frac{\partial \overline{u_i'u_j'w'}}{\partial t} = &-\overline{u_i'w'^2}\frac{\partial \overline{u_j}}{\partial z} - \overline{u_j'w'^2}\frac{\partial \overline{u_i}}{\partial z} - \overline{w'^2}\frac{\partial \overline{u_i'u_j'}}{\partial z} - \overline{u_j'w'}\frac{\partial \overline{u_i'w'}}{\partial z} - \overline{u_i'w'}\frac{\partial \overline{u_j'w'}}{\partial z} \\ &+ \beta\left(\overline{u_i'u_j'T'} + \overline{u_i'w'T'}\delta_{3j} + \overline{u_j'w'T'}\delta_{3i}\right) - c_8\frac{\varepsilon}{\overline{e}}\overline{u_i'u_j'w'}\end{aligned} \tag{9}$$

$$\left|\overline{u_i'u_j'w'}\right| \le \min\left\{\begin{matrix}\left[u_i'^2\left(\overline{u_j'^2}\cdot\overline{w'^2} + \overline{u_j'w'}^2\right)\right]^{1/2} \\ \left[u_j'^2\left(\overline{u_i'^2}\cdot\overline{w'^2} + \overline{u_i'w'}^2\right)\right]^{1/2} \\ \left[w'^2\left(\overline{u_i'^2}\cdot\overline{u_j'^2} + \overline{u_i'u_j'}^2\right)\right]^{1/2}\end{matrix}\right\} \tag{10}$$

$$\begin{aligned}\frac{\partial \overline{u_i'u_j'T'}}{\partial t} = &-\overline{u_i'u_j'w'}\frac{\partial \overline{T}}{\partial z} - \overline{u_i'w'T'}\frac{\partial \overline{u_j}}{\partial z} - \overline{u_j'w'T'}\frac{\partial \overline{u_i}}{\partial z} - \overline{w'T'}\frac{\partial \overline{u_i'u_j'}}{\partial z} - \overline{u_i'w'}\frac{\partial \overline{u_j'T'}}{\partial z} \\ &- \overline{u_j'w'}\frac{\partial \overline{u_i'T'}}{\partial z} + \beta\left(\overline{u_i'T'^2}\delta_{3j} + \overline{u_j'T'^2}\delta_{3i}\right) - c_8\frac{\varepsilon}{\overline{e}}\left(\overline{u_i'u_j'T'} - \frac{1}{3}\delta_{ij}\overline{u_k'u_k'T'}\right) \\ &+ c_9\frac{\varepsilon}{\overline{e}}\delta_{ij}\overline{u_k'u_k'T'} - \frac{1}{3}c_{10}\frac{\varepsilon}{\overline{e}}\delta_{ij}\overline{u_k'u_k'T'}\end{aligned} \tag{11}$$

$$\left|\overline{u_i'u_j'T'}\right| \le \min\left\{\begin{matrix}\left[u_i'^2\left(\overline{u_j'^2}\cdot\overline{T'^2} + \overline{u_j'T'}^2\right)\right]^{1/2} \\ \left[u_j'^2\left(\overline{u_i'^2}\cdot\overline{T'^2} + \overline{u_i'T'}^2\right)\right]^{1/2} \\ \left[T'^2\left(\overline{u_i'^2}\cdot\overline{u_j'^2} + \overline{u_i'u_j'}^2\right)\right]^{1/2}\end{matrix}\right\} \tag{12}$$

$$\begin{aligned}\frac{\partial \overline{u_i'T'^2}}{\partial t} = &-\overline{w'T'^2}\frac{\partial \overline{u_i}}{\partial z} - 2\overline{u_i'w'T'}\frac{\partial \overline{T}}{\partial z} - \overline{u_i'w'}\frac{\partial \overline{T'^2}}{\partial z} - 2\overline{w'T'}\frac{\partial \overline{u_i'T'}}{\partial z} \\ &+ \beta\overline{T'^3}\delta_{3i} - c_8\frac{\varepsilon}{\overline{e}}\overline{u_i'T'^2}\end{aligned} \tag{13}$$

$$\left|\overline{u_i'T'^2}\right| \le \left[\overline{T'^2}\left(\overline{u_i'^2}\cdot\overline{T'^2} + \overline{u_i'T'}^2\right)\right]^{1/2} \tag{14}$$

$$\frac{\partial \overline{T'^3}}{\partial t} = -3\overline{w'T'^2}\frac{\partial \overline{T}}{\partial z} - 3\overline{w'T'}\frac{\partial \overline{T'^2}}{\partial z} - c_{10}\frac{\varepsilon}{\overline{e}}\overline{T'^3} \tag{15}$$

$$\left|\overline{T'^3}\right| \le \left(2\overline{T'^2}^3\right)^{\frac{1}{2}}. \tag{16}$$

In these equations $e = \frac{1}{2}u_i'u_i'$ and $\overline{e} = \frac{1}{2}\overline{u_i'u_i'}$. The model coefficients are given as:

$$\begin{aligned} &a_1 = 0.15; \quad a_2 = 1.44; \quad a_{2T} = 0.7; \quad a_3 = 1.9; \\ &c_2 = 2.7; \quad c_4 = 4.5, \quad c_5 = 0; \quad c_6 = 4.85; \\ &c_7 = 0.394; \quad c_8 = 8.5, \quad c_9 = -1.5; \quad c_{10} = 4. \end{aligned} \tag{17}$$

Asymmetric Channel Flows

The example of asymmetric channel flow as described by Andre et al (1979) is discussed in this section. The mean velocity and turbulent shear stress are compared with the experimental data in Figure 1 and good agreement is observed. Figure 2 compares the predicted mean fluctuation energy and the dissipation rate with the experimental data. While there are some differences, the general agreement with the data is reasonable.

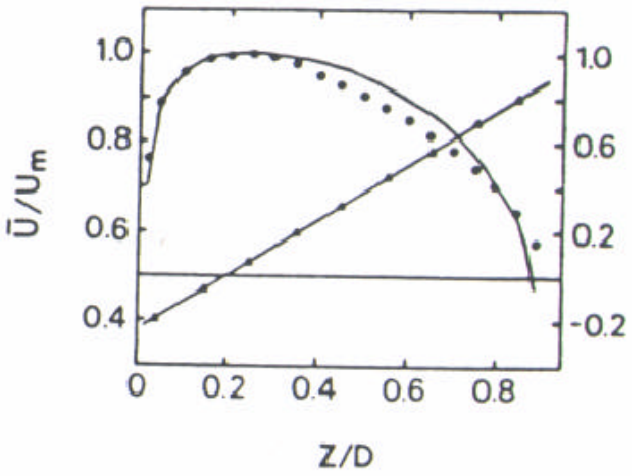

Figure 1. Comparison of mean velocity and shear stress profiles with experimental data.

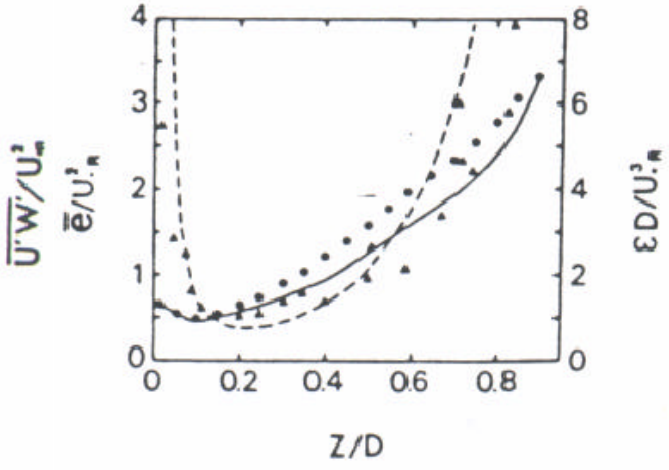

Figure 2. Comparison of turbulence kinetic energy and dissipation rate profiles with experimental data.

Variations of the some third order moments across the channel as predicted by the clipping approximation are shown in Figures 3 and 4. The experimental data for the corresponding moments are also plotted in Figure 3 and 4 for comparison. These figures show that the general agreement is quite reasonable.

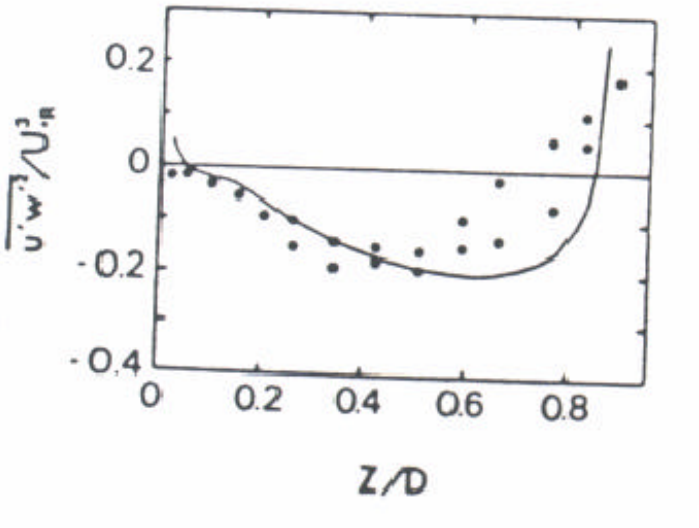

Figure 3. Comparison of third order moment with experimental data.

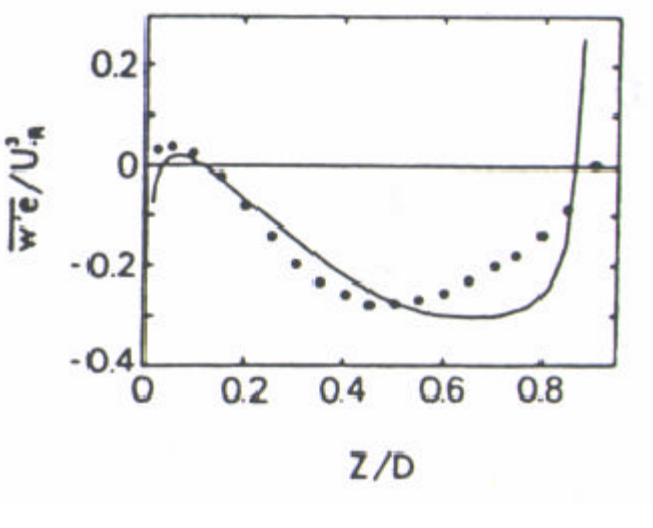

Figure 4. Comparison of third order moment with experimental data.

Lin and Wolfshtein (Two-point Double Velocity Correlation) (1979)

Lin and Woldshtein (1979) examined the Reynolds stress transport equation given as

$$\frac{D}{Dt}\overline{u_i'u_j'} = -\left(\overline{u_i'u_k'}\frac{\partial U_j}{\partial x_k} + \overline{u_j'u_k'}\frac{\partial U_i}{\partial x_k}\right) - \frac{\partial}{\partial x_k}\overline{u_i'u_j'u_k'} - \frac{1}{\rho}\left(\overline{u_i'\frac{\partial p'}{\partial x_j} + u_j'\frac{\partial p'}{\partial x_i}}\right) + \nu\left(\frac{\partial^2\overline{u_i'u_j'}}{\partial x_k\partial x_k} - 2\overline{\frac{\partial u_i'}{\partial x_k}\frac{\partial u_j'}{\partial x_k}}\right) \tag{18}$$

The pressure gradient-velocity correlation is given by

$$P_{ij} = -\frac{1}{\rho}\left(\overline{u_i'\frac{\partial p'}{\partial x_j} + u_j'\frac{\partial p'}{\partial x_i}}\right) \tag{19}$$

Noting that

$$\nabla^2\frac{p'}{\rho} = -(S_1 + S_2), \qquad S_1 = 2\frac{\partial U_\ell}{\partial x_k}\frac{\partial u_k'}{\partial x_\ell}, \qquad S_2 = \frac{\partial^2}{\partial x_k\partial x_\ell}\left(u_k'u_\ell' - \overline{u_k'u_\ell'}\right) \tag{20}$$

then

$$\frac{p'}{\rho} = \frac{1}{4\pi}\int_V GS_1 dV + \int_V GS_2 dV \tag{21}$$

where G is the Green function. Using (21), the pressure gradient –velocity correlation given by Equation (19) may be restated as

$$P_{ij} = P_{ij_1} + P_{ij_2} + P_{ij_3} + P_{ij_4} \tag{22}$$

where

$$P_{ij_1} = \frac{2}{3}\left(\overline{u_i'u_k'}\frac{\partial U_j}{\partial x_k} + \overline{u_j'u_k'}\frac{\partial U_i}{\partial x_k}\right) \qquad \text{(Forced Interaction)} \tag{23}$$

$$P_{ij_2} = -\frac{1}{2\pi}\int_V \frac{\partial U_k(B)}{\partial r_\ell}\left(Q_{j\ell}\frac{\partial G}{\partial r_k\partial r_\ell} + Q_{i\ell}\frac{\partial^2 G}{\partial r_k\partial r_j}\right)dV \qquad \text{(Forced Interaction)} \tag{24}$$

$$P_{ij_3} = \frac{1}{3}\left(\frac{\partial S_{ikk}}{\partial x_j} + \frac{\partial S_{jkk}}{\partial x_i}\right) \qquad \text{(Free Interaction)} \tag{25}$$

$$P_{ij_4} = \frac{1}{4\pi}\int_V \left(S_{i,k\ell}\frac{\partial^3 G}{\partial r_k \partial r_\ell \partial r_j} + S_{j,k\ell}\frac{\partial^3 G}{\partial r_k \partial r_\ell \partial r_i}\right) dV \qquad \text{(Free Interaction)} \tag{26}$$

Here,

$$S_{ik\ell} = \overline{u_i' u_k' u_\ell'}\,,\ S_{i,k\ell} = \overline{u_i'(A) u_k'(B) u_\ell'(B)}\,. \tag{27}$$

Note that P_{ij_4} is a volume integral of the triple-velocity two-point correlation tensor. For isotropic turbulence, it may be shown that

$$P_{ij_4} = -2\left(\frac{2k}{3}\right)^{\frac{3}{2}}\delta_{ij}\int_0^\infty \frac{1}{r}\frac{dh}{dr}dr \quad (h \text{ - isotropic triple-velocity correlation}) \tag{28}$$

It is assumed that

$$P_{ij_4} = P_{ij_{41}} + P_{ij_{42}} = \text{Dissipation} + \text{Diffusion} \tag{29}$$

The dissipation part is given as

$$P_{ij_{41}} = -\Lambda_1 \frac{\nu k}{\lambda^2}\left(1 + \alpha_2 R_T\right), \tag{30}$$

where Λ_1, α_2 are constants and

$$R_T = k^{\frac{1}{2}}\frac{\lambda}{\nu} \tag{31}$$

Lin and Woldshtein (1979) suggested the following closure assumption for the two-point double velocity correlation:

$$Q_{ij}(\mathbf{x},\mathbf{r}) = \frac{3}{2k} R_{rs}(\mathbf{x}) R_{pt}(\mathbf{x}+\mathbf{r}) g_{rsptij}(\mathbf{x}, r) \tag{32}$$

with

$$R_{rs}(x) = \overline{u_r' u_s'}\,, \qquad Q_{ij} = \overline{u_i'(x) u_j'(\mathbf{x}+\mathbf{r})}\,. \tag{33}$$

Here, g_{rsptij} is an isotropic sixth-order tensor.

The expression for the forced interaction term, P_{ij_2}, is given as

$$P_{ij_2} = A\pi_{ij} + B\tilde{D}_{ij} + C\frac{\pi_{\ell\ell}}{3}\delta_{ij} + E\frac{4k}{3}D_{ij}, \qquad A + B + C = \frac{2}{3} \tag{34}$$

where

$$\tilde{D}_{ij} = -\left(R_{ik}\frac{\partial U_k}{\partial x_j} + R_{jk}\frac{\partial U_k}{\partial x_i}\right), \qquad D_{ij} = \frac{1}{2}\left(\frac{\partial U_i}{\partial x_j} + \frac{\partial U_j}{\partial x_i}\right) \tag{35}$$

The last two terms in Equation (18) are the viscous diffusion and the dissipation terms. These are given as

$$\varepsilon_{ij_1} = \nu\frac{\partial^2 R_{ij}}{\partial x_k \partial x_k}, \qquad \varepsilon_{ij_2} = -2\nu\overline{\frac{\partial u_i'}{\partial x_j}\frac{\partial u_i'}{\partial x_j}} \tag{36}$$

The dissipation is given as

$$\varepsilon_{ij_2} = 2\nu\nabla_r^2 Q_{ij}\,|_{r=0} = -2\nu M_{ij} \tag{37}$$

Here M_{ij} is related to the derivative of two-point double velocity correlation tensor and satisfies the following transport equation:

$$\frac{D}{Dt}M_{ij} = A_1\left(M_{ik}\frac{\partial U_j}{\partial x_k} + M_{jk}\frac{\partial U_i}{\partial x_k}\right) + e_5\frac{\nu}{\lambda_3^2}M_{ij}\left(1 + e_3 R_T\right) \tag{38}$$

where

$$A = -1.642, \quad e_3 = 3.6 \tag{39}$$

The final transport equation used by Lin and Woldshtein (1979) is given as

$$\begin{aligned}\frac{D}{Dt}R_{ij} = &-\left(R_{ik}\frac{\partial U_j}{\partial x_k} + R_{jk}\frac{\partial U_i}{\partial x_k}\right)\left(A + \frac{1}{3}\right) + B\tilde{D}_{ij} - \frac{2C}{3}R_{\ell k}\frac{\partial U_\ell}{\partial x_k}\delta_{ij} + E\frac{4k}{3}D_{ij} \\ &- \frac{\partial S_{ijk}}{\partial x_k} + \frac{1}{3}\left(\frac{\partial \delta_{ikk}}{\partial x_j} + \frac{\partial \delta_{jkk}}{\partial x_i}\right) + P_{ij41} + \nu\frac{\partial^2 R_{ij}}{\partial x_k \partial x_k} - GR_{ij} - \frac{2}{3}kH\delta_{ij}\end{aligned} \tag{40}$$

Here

$$G = \frac{20\Lambda}{3}(1+\alpha R_T)\frac{\nu}{\lambda_1^2}, \qquad H = \left[\frac{3\Lambda_2}{2}(1+\alpha R_T)+\frac{20}{3}(1-\Lambda)(1+\alpha R_T)\right]\frac{\nu}{\lambda_1^2} \tag{41}$$

The simulation results of Lin and Woldshtein (1979) are shown in Figures 5-8. Figure 5 compare the predicted turbulence normal and shear stresses, $\tilde{U}_{ij} = \overline{u_i' u_j'}$, in a homogenous shear flow with the experimental data of Champagne et al. (1971). It is seen that the axial component of normal stress is about twice the stresses in the other directions. The model prediction is also in good agreement with the experimental data.

Comparison of the predicted turbulence intensities in a contracting duct with the experimental data of Uberoi and Wallis is shown in Figure 6. It is seen that the model captures the features of the experimental quite well. This figure also shows that the contraction tends to make the turbulence fluctuation more isotropic.

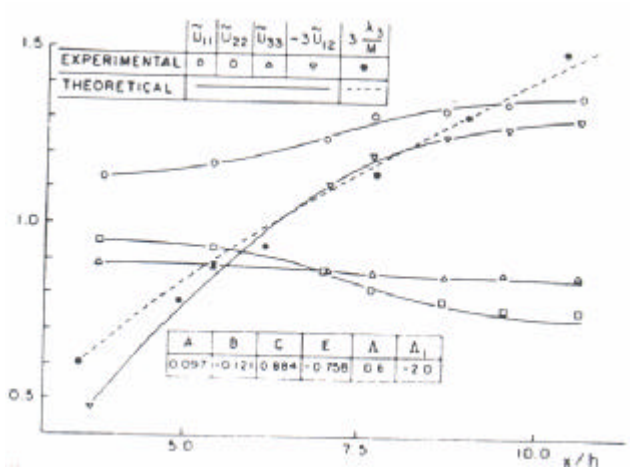

Figure 5. Comparison of the predicted turbulence intensities and scales in homogenous shear flows with the experimental data of Champagne et al. (1971).

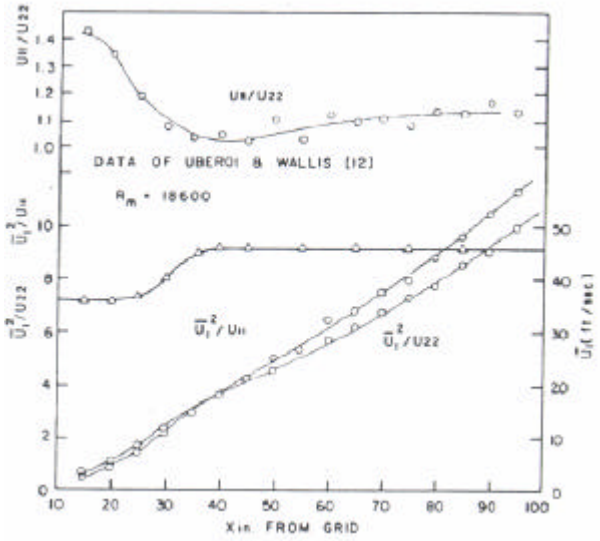

Figure 6. Comparison of the predicted turbulence intensities in a contracting duct with the experimental data of Uberoi and Wallis.

Variations of the ratio U_{11}/U_{22} with mesh Reynolds number in a contracting ducts are shown in Figure 7. The experimental data of Uberoi and Wallis is also shown in this figure for comparison. It is seen that the model predictions are in good agreement with the data.

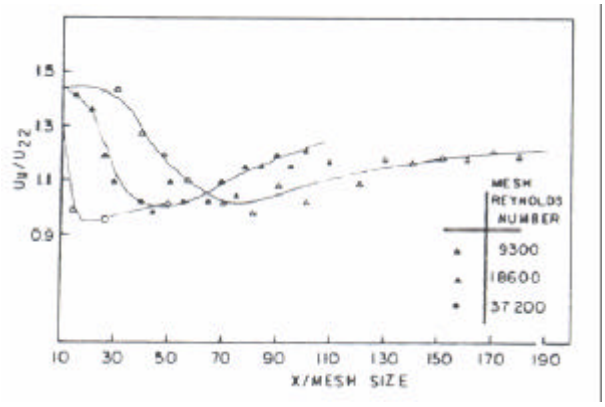

Figure 7. Comparison of the effect of mesh Reynolds on turbulence intensity ratios, with the experimental data of Uberoi and Wallis.

The variations of the Reynolds stress distribution for a plane strain flows are listed in Table 1. Here the mean strain is defined as

$$\overline{e_{ij}} = \frac{1}{2}\left(\frac{\partial \overline{U_i}}{\partial x_j} + \frac{\partial \overline{U_j}}{\partial x_i}\right). \tag{42}$$

Table 1. Reynolds stress distribution in plane strain flow.

$\overline{e}_{11}$	$\overline{e}_{22}$	$\overline{e}_{33}$	$\tilde{U}_{11}$	$\tilde{U}_{22}$	$\tilde{U}_{33}$
0	**4.45**	**-4.45**	**1.85**	**0.35**	**0.70**
2.6	**2.6**	**-5.2**	**0.57**	**0.93**	**1.50**
-1.3	**2.6**	**-1.3**	**0.48**	**1.36**	**1.36**

Comparison of the predicted variations of the turbulence intensities in a uniformly strained flow with the experimental data of Reynolds and Tucker is shown in Figure 8. Here a range strain ratio is used. It is seen that the intensities decrease with the increase in the strain ratio and the distance form the virtual origin. The model predictions are also in good agreement with the experimental data.

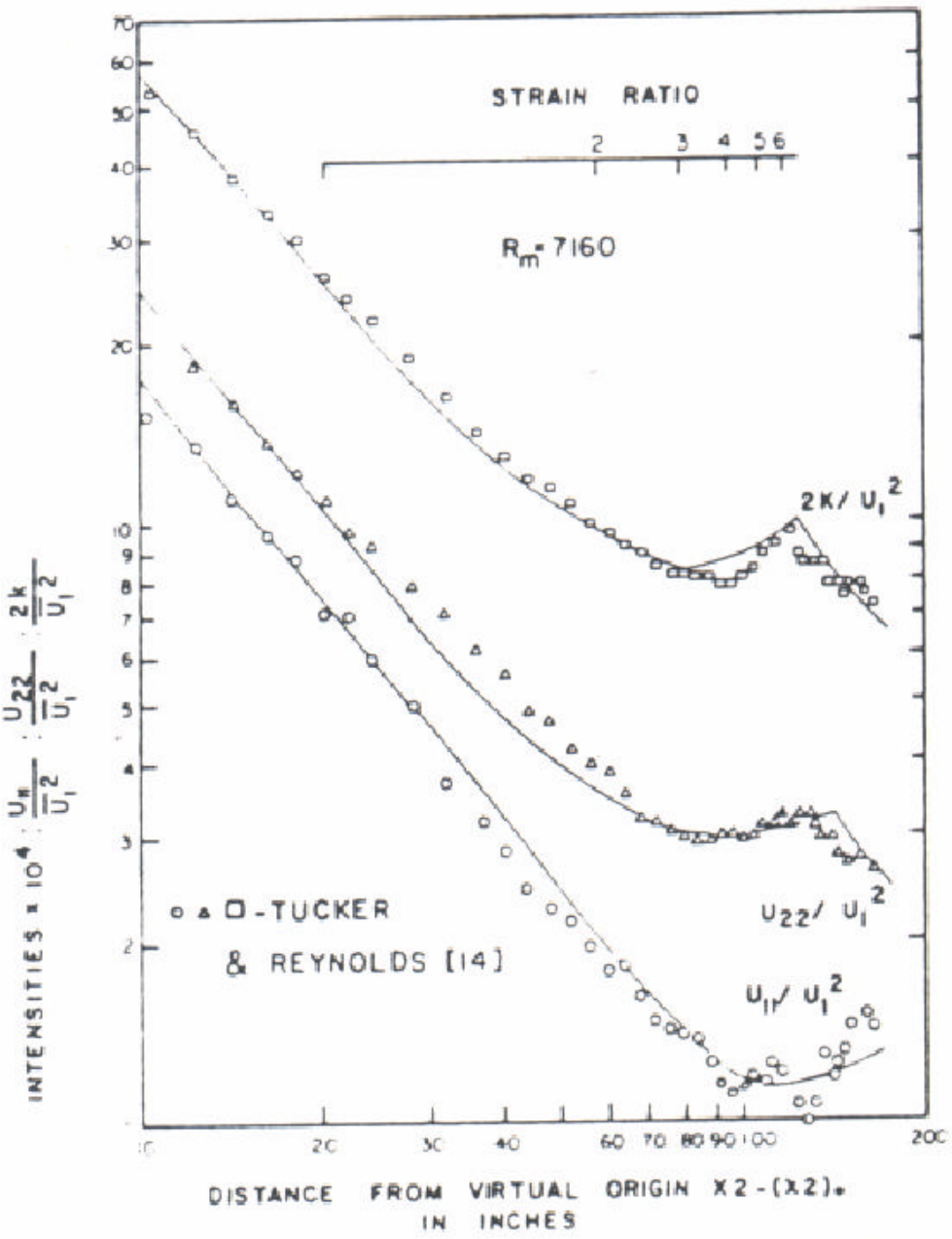

Figure 8. Comparison of the predicted turbulence intensities in uniformly strained flows with the experimental data of Reynolds and Tucker.

Multiple-Time-Scale Concepts in Turbulent Transport Modeling (Hanjalic, Launder, and Schiestel) (1980)

Most common stress closure models use a single time scale $\frac{k}{\varepsilon}$. Thus, processes are assumed to occur at a rate proportional to $\frac{\varepsilon}{k}$, but this assumption may be too restrictive in many applications. Hanjalic et al. (1980) introduced the multiple time scale model. They noted that the energy spectrum of turbulence may be divided into different parts are shown in Figure 9. Here the subscript p denotes production and T identifies transport.

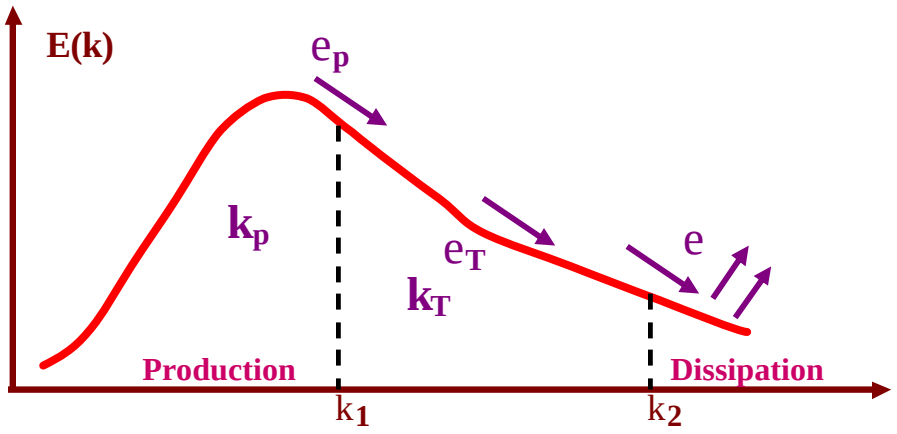

Figure 9. Schematics of turbulence energy spectrum.

Let

$$k \approx k_p + k_T \tag{43}$$

For homogenous flows, the transport equations for k_p and k_T are then give as

$$\frac{Dk_P}{Dt} = -\overline{u_i' u_j'} \frac{\partial U_i}{\partial x_j} - \varepsilon_P \tag{44}$$

$$\frac{Dk_T}{Dt} = \varepsilon_P - \varepsilon \tag{45}$$

The transport equations for ε_p and ε_p are given by

$$\frac{D\varepsilon_P}{Dt} = c_{P1} P_k \frac{\varepsilon_P}{k_P} - c_{P2} \frac{\varepsilon_P^2}{k_P} + D_{\varepsilon P}, \tag{46}$$

$$\frac{D\varepsilon_T}{Dt} = c_{T1} \frac{\varepsilon_P \varepsilon_T}{k_T} - c_{T2} \frac{\varepsilon_T^2}{k_T} + D_{\varepsilon T}, \tag{47}$$

where $D_{\varepsilon P}$, $D_{\varepsilon T}$ being diffusive transport and $P_k = -\overline{u_i' u_j'} \frac{\partial U_i}{\partial x_j}$ is the turbulence kinetic energy production. The model parameters are given as

$$\varepsilon = \varepsilon_T, \quad c_{P_1} = 2.2, \quad c_{P_2} = 1.8 - 0.3 \frac{\frac{k_P}{k_T} - 1}{\frac{k_P}{k_T} + 1}, \quad C_{T_1} = 1.08 \frac{\varepsilon_P}{\varepsilon_T} \tag{48}$$

$$C_{T_2} = 1.15, \quad D_\varphi = 0.22 \frac{\partial}{\partial x_k} \left(\overline{u_k' u_\ell'} \frac{k_P}{\varepsilon_P} \frac{\partial \varphi}{\partial x_k} \right), \quad \varphi \sim k_P, \; k_T, \; \varepsilon_P, \; \varepsilon_T \tag{49}$$

The corresponding "Stress Transport Equation" is given as

$$\frac{D}{Dt} \overline{u_i' u_j'} = \left\{ \begin{array}{l} -\left(\overline{u_i' u_k'} \frac{\partial U_j}{\partial x_k} + \overline{u_j' u_k'} \frac{\partial U_i}{\partial x_k} \right) - \frac{2}{3} \delta_{ij} \varepsilon - 1.5 \frac{\varepsilon_P}{k_P} \left(\overline{u_i' u_j'} - \frac{2}{3} k \delta_i \right) + \varphi_{ij_2} \\ + \varphi_{ij_w} + 0.11 \frac{\partial}{\partial x_k} \left[\frac{k_P}{\varepsilon_P} \left(\overline{u_P' u_k'} \frac{\partial \overline{u_i' u_j'}}{\partial x_\ell} + \overline{u_\ell' u_j'} \frac{\partial \overline{u_k' u_i'}}{\partial x_\ell} + \overline{u_P' u_i'} \frac{\partial \overline{u_k' u_j'}}{\partial x_\ell} \right) \right] \end{array} \right\} \tag{50}$$

Hanjalic et al. (1980) studied uniformly strained turbulence, axisymmetric jets, and boundary layer flows with adverse pressure gradient. Their results are summarized in this section.

Strained Turbulent Flows

Figure 10 compares variations of turbulence kinetic energy as predicted by the single and double-scale models with the experimental data for contraction ratio of 4:1. It is seen that the double-scale model improves the agreement of the model prediction with the experiment. Variations of k_p and k_T are also shown in this figure for comparison. This figure shows that k_p follows the same trend as k but at lower amplitude; k_T, however, exhibit smaller variation in its amplitude.

Variations of energy transfer rates are shown in Figure 11. It is seen that ε_p follows a trend similar to k_p, and ε_T has larger values at the short distances, but becomes comparable to ε_p at larger distances.

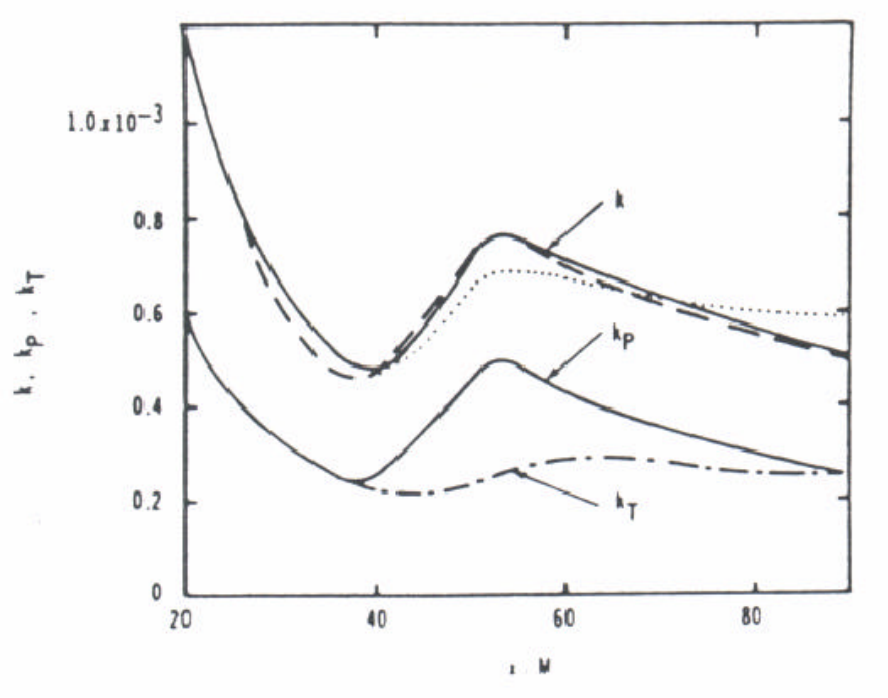

Figure 10. Variation of kinetic energies in a contraction. ------ experiment; …… single scale; _____ double scale.

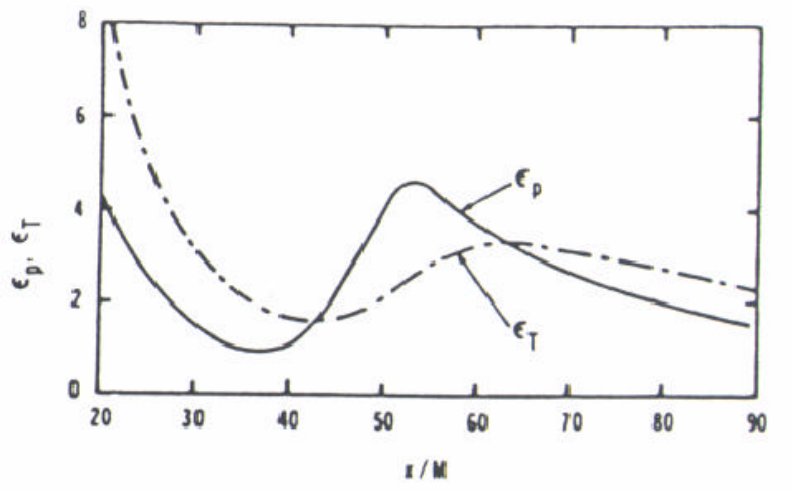

Figure 11. Variation of energy transfer rates in a 4:1 contraction.

Turbulence Plane Jet

Model predictions for a turbulence plane jet are shown in Figure 12. The experimental data of Robins (1972) for the mean velocity and Bradbury (1965) for turbulence kinetic energy are reproduced in this figure for comparison. It is seen that the double-scale model predictions are in good agreement with the experimental data.

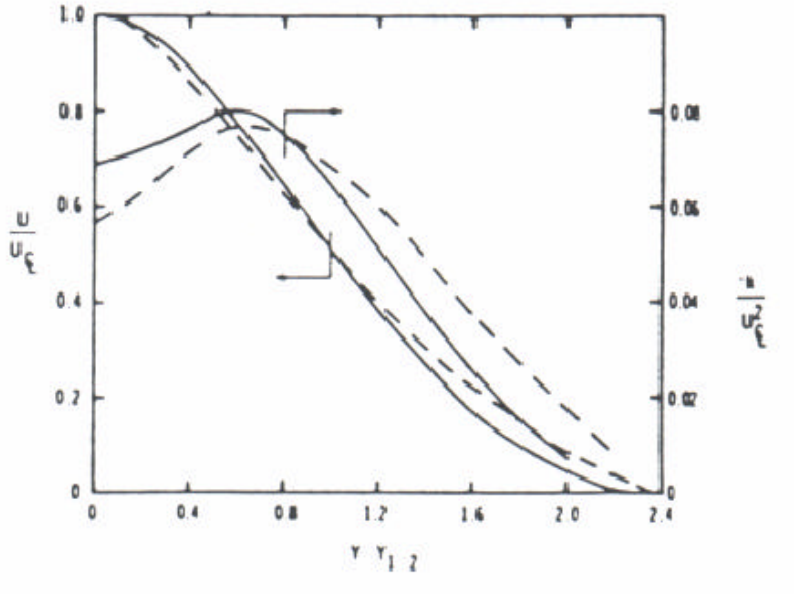

Figure 12. Variation of mean velocity and turbulence kinetic energy in a plane turbulent jet flow. ------ double scale; _____experiment.

The predicted rate of growth of the half widths of round and plane jets are compared with the experimental data in Table 2. It is seen that the multi-scale model predictions are in good agreement with the experimental data.

Table2. Rate of growth of half widths of round and plane jets

Flow	Experiment	Single-Scale	Double-Scale
Plane Jet	**0.11**	**0.109**	**0.116**
Axisymmetric Jet	**0.086-0.090**	**0.115**	**0.098**

Boundary Layer Flows with Adverse Pressure Gradients

Hanjalic et al. (1980) used the double-scale model in their analysis of boundary layer flows with adverse pressure gradient. The corresponding variations of the skin friction coefficient and the pressure gradient parameters are shown in Figure 13. The experimental data of Bradshaw (1969) and the single-scale model predictions of Launder et al. (1975) are also reproduced in this figure for comparison. The marked improvement of the model predictions with the use of double-scale model can be clearly seen from Figure 13.

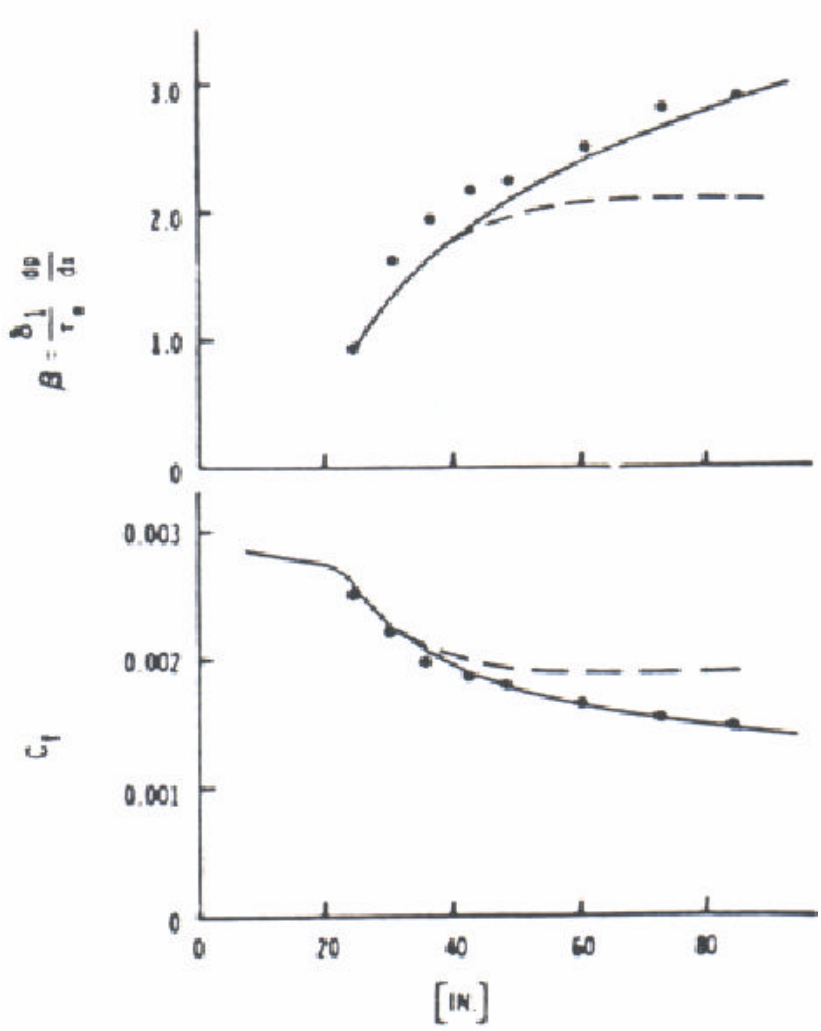

Figure 13. Variation of skin friction coefficient and the pressure gradient parameters in a turbulent boundary layer flow with adverse pressure gradient. _____ double-scale; ------Single-scale, Launder et al. (1975); • experiment, Bradshaw (1969) .

The predicted variation of mean velocity and turbulence shear stress in a turbulent boundary layer flow with adverse pressure gradient are shown in Figure 14. The experimental data of Bradshaw (1969) are also shown in this figure for comparison. It is seen that the double–scale model well predicts the experimental data.

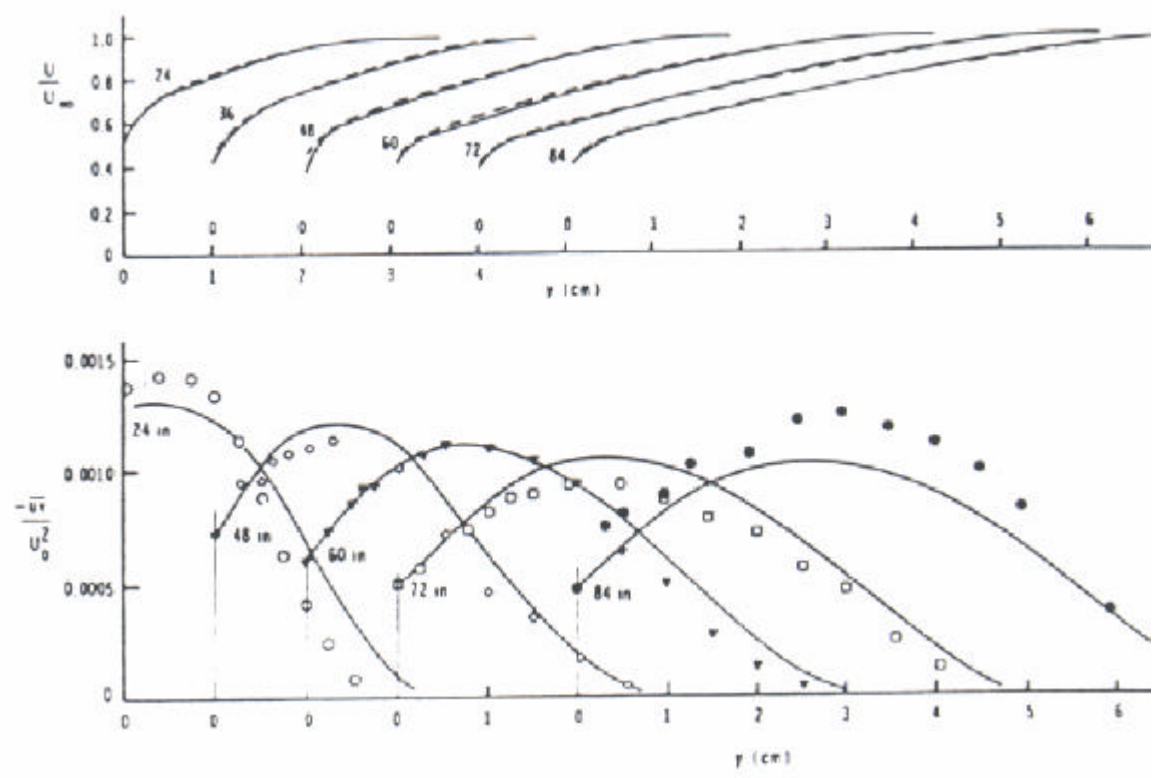

Figure 14. Variation of mean velocity and turbulence shear stress in a turbulent boundary layer flow with adverse pressure gradient. Comparison with the experimental data of Bradshaw (1969).